

Article

# A Concise and Adaptive Sidelobe Suppression Algorithm Based on LMS Filter for Pulse-Compressed Signal of $\Phi$ -OTDR

Wei Shen<sup>1</sup>, Xiaofeng Chen<sup>2</sup>, Yong Zhang<sup>1</sup>, Xin Hu<sup>1</sup>, Jian Wu<sup>1</sup>, Lijun Liu<sup>1</sup>, Chuanlu Deng<sup>2</sup>, Chengyong Hu<sup>2</sup> and Yi Huang<sup>2,\*</sup> 

<sup>1</sup> China State Grid Taizhou Power Supply Company, Taizhou 225300, China; shenwei5630@vip.sina.com (W.S.); zhangyong@cloud-intelligent.com (Y.Z.); tzhuxin@foxmail.com (X.H.); jianwu102405@163.com (J.W.); liulijun02@163.com (L.L.)

<sup>2</sup> Key Laboratory of Specialty Fiber Optics and Optical Access Networks, Shanghai University, Shanghai 200444, China; xiaofeng1021@shu.edu.cn (X.C.); 13820256@shu.edu.cn (C.D.); hu516615784@shu.edu.cn (C.H.)

\* Correspondence: huangyi1008@shu.edu.cn

**Abstract:** A concise and adaptive sidelobe suppression algorithm based on a least mean square (LMS) filter is proposed for pulse-compressed signals of a phase-sensitive optical time-domain reflectometer ( $\Phi$ -OTDR) system. The algorithm is suitable for the denoising filtering process of phase coding OTDR (PC-OTDR) systems and mitigates the sidelobe effect due to matched filtering. In a simulation experiment, Rayleigh backscattering (RBS) signals including phase-coded pulse signals are generated and decoded to verify that the LMS algorithm can eliminate the sidelobes more effectively than the windowing method and the recursive least squares (RLS) method. Then, the PC-OTDR system is set up and combined with the LMS algorithm for positioning experiments. The results show that the peak side lobe ratio (PSLR) of the signals can reach  $-15.86$  dB, which is  $4.26$  dB lower than the raw pulse compressed signal.

**Keywords:** optical time domain reflectometer system; pulse compression; adaptive filtering; sidelobe suppression



**Citation:** Shen, W.; Chen, X.; Zhang, Y.; Hu, X.; Wu, J.; Liu, L.; Deng, C.; Hu, C.; Huang, Y. A Concise and Adaptive Sidelobe Suppression Algorithm Based on LMS Filter for Pulse-Compressed Signal of  $\Phi$ -OTDR. *Photonics* **2024**, *11*, 70. <https://doi.org/10.3390/photonics11010070>

Received: 14 November 2023

Revised: 2 January 2024

Accepted: 6 January 2024

Published: 8 January 2024



**Copyright:** © 2024 by the authors. Licensee MDPI, Basel, Switzerland. This article is an open access article distributed under the terms and conditions of the Creative Commons Attribution (CC BY) license (<https://creativecommons.org/licenses/by/4.0/>).

## 1. Introduction

The phase-sensitive optical time-domain reflectometer ( $\Phi$ -OTDR) is a fully distributed optical fiber sensing technology [1], which is widely applied in rail transportation safety monitoring [2], smart grid condition monitoring [3], infrastructure perimeter security [4], and so on. Conventional  $\Phi$ -OTDR systems have inevitable limitations, mainly in the trade-off between dynamic range and spatial resolution. Good spatial resolution requires narrow probe pulses, which limits detection sensitivity due to attenuation [5]. Therefore, the improvement of the performance of the  $\Phi$ -OTDR system while ensuring the dynamic range and spatial resolution remains an urgent problem.

In order to meet these challenges, an effective method using the pulse compression technique to realize the modulation and demodulation of probe pulses is proposed [6–8]. Pulse compression technique is a commonly used radar detection enhancement technique, which is used to interconvert broadband signals into narrowband signals, and can change the time width and frequency bandwidth of the signal without changing the signal energy. In  $\Phi$ -OTDR systems, the pulse compression technique can be realized by encoding the probe pulse at the transmitter side and decoding the signals at the receiver side, which improves the dynamic range while maintaining a high spatial resolution [9–11].

Several OTDR systems based on pulse compression theory, such as linear frequency modulation [12], binary phase coding [13], and pseudo-random noise coding [14], have been proposed in recent years. Among them, the phase coding OTDR system (PC-OTDR) has a higher compression ratio and a lower peak side lobe ratio (PSLR), which enhances

spatial resolution and dynamic range. One of the key issues in PC-OTDR systems is the sidelobe effect. Sidelobes are the peaks or valleys formed by non-zero amplitude regions other than the main lobe in the pulse-compressed signal waveform obtained after decoding. The sidelobe effect will interfere with the pulse compression signal and distort its waveform, which affects the accuracy of the OTDR system in localizing the disturbed point. Therefore, finding a method to effectively suppress the sidelobe effect is the key to improving the measurement accuracy and stability of the PC-OTDR system. In 2013, the method of simple coded pulses instead of a single pulse was proposed for fiber break and loss detection, but the signal-to-noise ratio (SNR) improvement was only 3.7 dB due to the coding length limitation [15]. Compared to conventional amplitude shift keying (ASK) modulation, phase shift keying (PSK) has a higher bandwidth utilization in communication and high immunity-to-noise interference in sensing systems [16]. In 2016, H. F. Martins et al. employed a random and non-periodical PSK coded pulse in  $\Phi$ -OTDR and obtained the theoretical spatial resolution of 2.5 cm, but the system requires demanding environments such as low phase drift and static fiber [17]. In 2018, L. Shiloh et al. used 61,627-bit pseudorandom m-sequences in  $\Phi$ -OTDR [18], but the length of the autocorrelated pseudorandom code impact on the effect of suppressed sidelobes. Due to the long sequence period, the frequency range of detection is limited. The researchers mentioned above encoded the pulse at the transmitter side by changing the code pattern to reduce the amplitude of sidelobes. However, the sidelobe effect still exists due to the calculation of autocorrelation at the demodulation time, so a back-end sidelobe suppression algorithm for the scattering signals at the receiving end is necessary. In signal processing, due to the uncertainty of the perturbed signal and lack of a priori statistical information of the signal, an adaptive filter is critical for signal denoising and suppression of the sidelobes to prevent the sidelobes signal from generating interference that can lead to mispositioning.

In this work, a concise and adaptive sidelobe suppression algorithm based on the least mean square (LMS) filter is proposed. Firstly, the phase-coding modulation and matched filtering are theoretically analyzed. Based on this, the LMS adaptive filtering algorithm is applied to achieve sidelobe suppression to improve the SNR. In the simulation experiments, two sidelobe suppression methods (the windowing method and the recursive least squares (RLS) method) are compared, which demonstrates that the proposed method can improve the PSLR while maintaining a high spatial resolution. After building the real system, as expected, the SNR of the signal is significantly improved. Finally, the PC-OTDR system with a detection range of 11 km achieves a spatial resolution of 3.81 m with a PSLR of  $-13.5$  dB.

## 2. Principle and Method

### 2.1. Phase Coding and Matched Filtering Theory

In order to enhance the dynamic range of the system, a perturbation position scheme based on the pulse compression technique of an  $\Phi$ -OTDR system, which encodes the probe light into two phases ( $0$  or  $\pi$ ), is proposed. The schematic diagram of the system is shown in Figure 1. The system employs coherent detection where a narrow linewidth laser (NLL) is used to generate a highly coherent light source. The light source is divided into probe light and local light. The probe light is modulated by an electro-optic modulator (EOM) and is chopped by an acousto-optic modulator (AOM) into a two-phase encoded pulse. The modulated pulses are then injected into the fiber under test (FUT) through an optical circulator (OC) to generate Rayleigh backscattering (RBS) light and then beats the frequency with the local oscillator light, which enables coherent detection. In digital signal processing (DSP), the detected signal undergoes I/Q demodulation and then passes through a matched filter to be restored to the single pulse response. Finally, the intensity and phase signals can be obtained and used for subsequent signal filtering processes.

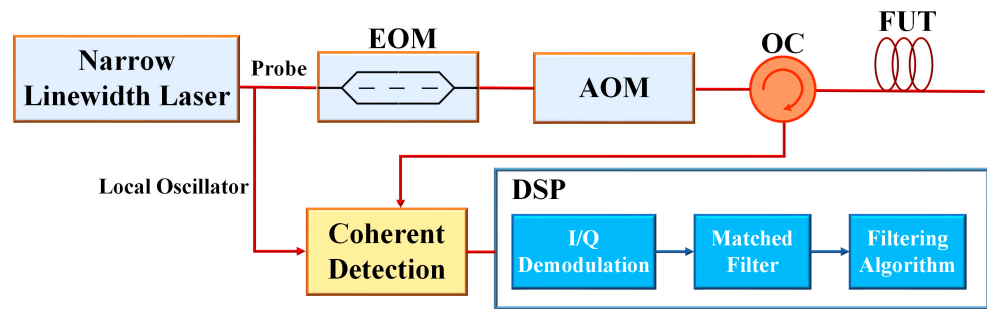


Figure 1. The schematic diagram of the PC-OTDR system.

In a PC-OTDR system, by periodically transmitting a sequence of probe pulses as the probe light, external perturbations acting on the optical fiber cause a change in the refractive index, thus changing the phase. The response of one probe pulse  $R(t)$  can be described as:

$$R(t) = A_s \exp(i\omega_s t + i\varphi_s + i\varphi(t)), \tag{1}$$

where  $A_s$ ,  $\omega_s$ , and  $\varphi_s$  are the amplitude, the angular frequency, and the initial phase of the signal, respectively. According to the linear time-invariant properties of the system, the coding sequence with  $M + 1$  bits can be shown as:

$$C = [C_0 \exp(i\varphi_0), C_1 \exp(i\varphi_1), \dots, C_M \exp(i\varphi_M)] \\ = [C_0, C_1 \exp(i\omega_s \tau), \dots, C_M \exp(i\omega_s M\tau)] \tag{2}$$

where  $C_p$  and  $\varphi_p$  ( $p = 0, 1, \dots, M$ ) are the amplitude and the phase of every code word, respectively. If the initial phase of the first code word of the pulse sequence is assumed to be the reference phase, and continuous phase-coded modulation is performed with a fixed time interval  $\tau$ , then the initial phase of each pulse can be determined. Based on Equation (2), assuming that the modulation signal is a sequence of rectangular pulses, the phase-coded modulation signal can be expressed as:

$$C(t) = \sum_{p=0}^M C_p \exp(i\omega_s p\tau) * \text{rect}\left(\frac{t - p\tau}{\tau}\right), \tag{3}$$

where  $p$  denotes the  $p$ -th subcode in the sequence, and  $\text{rect}(\cdot)$  denotes a rectangular signal. Based on Equations (1) and (3), after modulating the phase of the carrier frequency signal with a specific coding sequence, the modulated probe pulse signal can be obtained:

$$E(t) = R(t) * C(t) = A_s \sum_{p=0}^M C_p \exp[i\omega_s t + i\varphi(t - p\tau) + i\varphi_s] * \text{rect}\left(\frac{t - p\tau}{\tau}\right). \tag{4}$$

By adjusting the frequency shift and repetition frequency settings, the frequency band of the crosstalk signal is different from that of the useful signal. Specifically, an intermediate frequency (IF) signal can be obtained by eliminating the effect of crosstalk terms through outlier detection and bandpass filtering. After aforementioned operations and down-conversion,  $s(t)$  can be described as:

$$s(t) = C * \{A_l \cos[\varphi_l + \varphi(t)]\} = \sum_{p=0}^M C_p A_l \cos[\varphi_l + \varphi(t - p\tau)], \tag{5}$$

where  $A_l$  and  $\varphi_l$  are the adjusted amplitude and phase after bandpass filtering. In the

digital domain, the frequency response function  $h(t)$  of the matched filter is generated from the transmitted phase-coded signal;  $h(t)$  can be represented as:

$$h(t) = C^*(-t) = \sum_{p=0}^M C_p \exp(-i\omega_s p\tau) * \text{rect}\left(\frac{-t - p\tau}{\tau}\right). \quad (6)$$

The signal after matched filtering can be expressed as:

$$\begin{aligned} y(t) &= s(t) \otimes h(t) \\ &= \sum_{p=0}^M C_p A_l \cos[\varphi_l + \varphi(t - p\tau)] \otimes \sum_{p=0}^M C_p \exp(-i\omega_s p\tau) * \text{rect}\left(\frac{-t - p\tau}{\tau}\right), \end{aligned} \quad (7)$$

where  $\otimes$  denotes convolution. It can be seen that the result of the cross-correlation is the complex profile of the fiber convolved with the autocorrelation of the basic coded pulse.

One of the main considerations for the choice of code type is the relevance of the code. In the radar radio field, Barker codes are commonly used as a code type for pulse compression, but the limited length of Barker codes, up to 13 bits, makes it difficult to achieve high signal gain. After continuous research by scholars, Golay code is a pseudo-random sequence code that has good autocorrelation and low sidelobe properties, which is a suitable coding type for PC-OTDR [19]. The modulated RF signal applied to the EOM can be in the form of Golay codes, as shown in Figure 2a, which demonstrates the time-domain diagram of 128-bit non-return-to-zero (NRZ) Golay codes. In this encoding method, each bit occupies one clock cycle, corresponding to a single pulse width. Figure 2b shows the autocorrelation plot of this Golay pulse with ideally small sidelobes. However, the effect of sidelobes cannot be ignored due to random disturbances in real scenes. Big sidelobes not only deteriorate the spatial resolution but also can cause spurious peaks, which can lead to misjudgments.

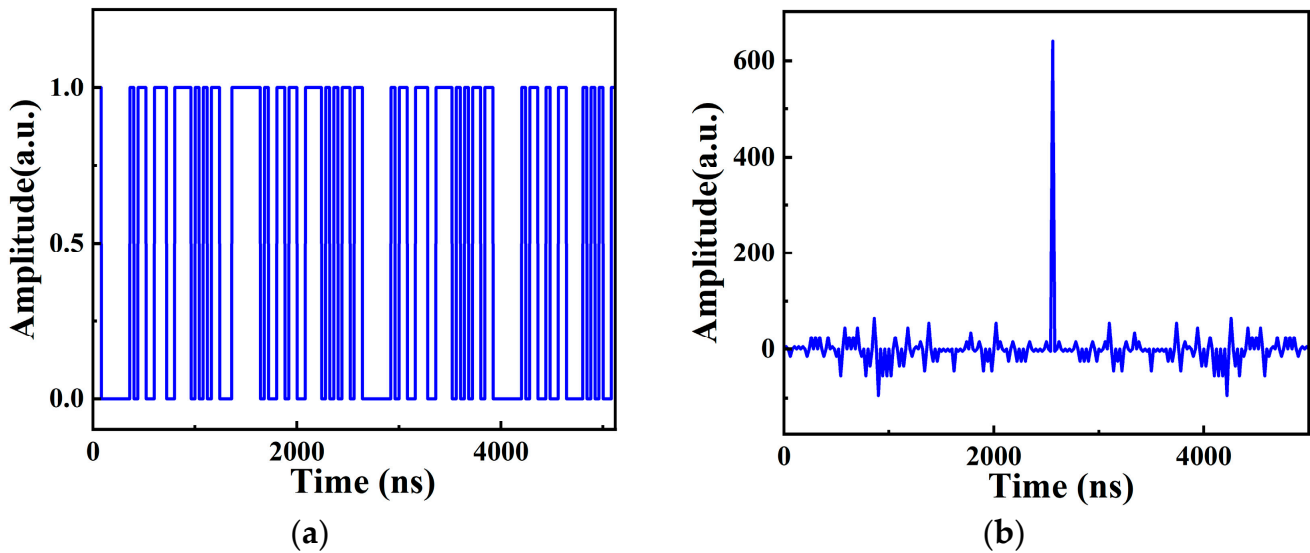


**Figure 2.** 128-bit Golay code signal. (a) Time domain signal, (b) autocorrelation function.

### 2.2. LMS Adaptive Filter

In the actual pulse compression process, the non-zero sidelobes can be considered as noise, and thus the filter can be designed according to the ideal matched-filter compression waveform to eliminate the noise. The LMS adaptive filter algorithm is a method to minimize the cost function based on the stochastic gradient descent technique, which has the advantages of low computational complexity, no need for prior knowledge of the statistical data, and unbiased convergence to the Wiener solution. It is one of the most widely used adaptive algorithms in signal processing. The adaptive noise reduction system based on

the LMS filter is shown in Figure 3. A signal is transmitted over a channel and is received by the receiver with uncorrelated noise  $x_0(n)$ . The signal  $s(n)$  and noise  $x_0(n)$  are combined to form the desired signal  $y(n) = s(n) + x_0(n)$ . A second signal input to the adaptive filter received by the secondary sensor is noise  $x(n)$ , which is uncorrelated with the signal but correlated with noise  $x_0(n)$ .

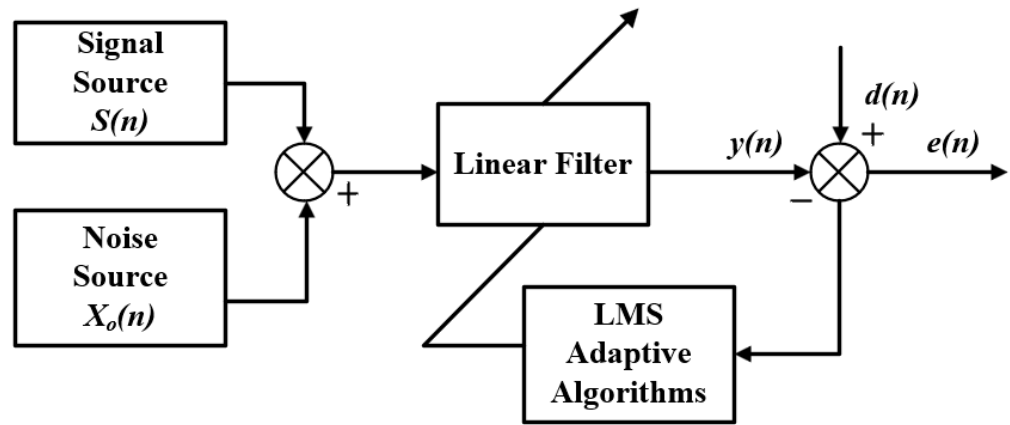


Figure 3. Schematic diagram of adaptive filtering system.

The LMS adaptive filter can be seen as a linear combiner with  $L + 1$  weights, which are denoted by a weight vector  $w(n) = [w_0(n), w_1(n), \dots, w_L(n)]^T$ . The input signal vector is  $s(n) = [s(n), s(n - 1), \dots, s(n - L)]^T$ . The output signal is:

$$y(n) = s^T(n) * w(n) = \sum_{k=0}^L w_k(n)s(n - k) \tag{8}$$

It is compared with the known signal  $d(n)$  to form the error signal  $e(n)$ . The error signal is:

$$e(n) = d(n) - y(n) = d(n) - s^T(n) * w(n) \tag{9}$$

The LMS algorithm uses an instantaneous gradient estimate to replace the exact gradient of the mean square error (MSE) function, and the weight vector of the LMS algorithm is updated as follows:

$$w(n + 1) = w(n) + 2\mu e(n)s(n), \tag{10}$$

where  $\mu$  is a step factor that controls the convergence speed and stability of the algorithm. The LMS algorithm step can be summarized as follows:

1. Initialize the weight vector  $w(0)$  and set a proper step factor  $\mu$ ;
2. For each new input sample  $s(n)$ , compute the output signal  $y(n)$  and the error signal  $e(n)$ ;
3. Update the weight vector  $w(n)$  according to the LMS update formula;
4. Repeat steps 1–2 until convergence or termination.

The LMS algorithm converges to the mean and the step size needs to be in range:

$$0 < \mu < \frac{2}{\lambda_{max}}, \tag{11}$$

where  $\lambda_{max}$  is the maximum eigenvalue of the correlation matrix. When the number of iterations approaches infinity, the adaptive filter coefficient vector  $w(n)$  is approximately equal to the optimal solution.

### 3. Simulations

#### 3.1. The Step Factor $\mu$ in the LMS Algorithm

The step factor  $\mu$  is one of the most important parameters of the LMS algorithm, which determines the convergence speed and stability of the algorithm. If the step size coefficient is not set appropriately, the convergence speed and stability will be greatly affected. When the step factor is large, the algorithm converges faster, while the single convergence error is large; when the step size is small, the algorithm will eventually converge to a small neighborhood near the Wiener solution, and the steady state error is small but the convergence speed is slow. In order to deal with the contradiction between convergence speed and steady state error, the step factor  $\mu$  can be adjusted to achieve the desired algorithm performance.

Based on the Sigmoid function, the step factor  $\mu$  that is nonlinearly curved reduces the speed of convergence and the error. Two parameters ( $\alpha$  and  $\beta$ ) are used to control the shape of the function and the amplitude of the function, respectively, thus controlling the speed and range of the step change. The step factor  $\mu(n)$  can be expressed as [20]:

$$\mu(n) = \beta \left( \frac{1}{1 + e^{(-\alpha|e(n)|)}} - 0.5 \right), \tag{12}$$

where  $\alpha$  and  $\beta$  are constant, which need to be preset.

In the simulation of parameter selection, the results of the error function and step factor with the constants  $\alpha$  or  $\beta$  are shown in Figure 4a,b. The value of  $\beta$  in Figure 4a serves only to limit the magnitude of the step factor. In Figure 4b, when  $\alpha = 5$ , the algorithm converges more quickly while the algorithm has a larger error in the initial stage, and the step size is also larger at this time. When the algorithm enters the steady state, the steady state mean square error will also be reduced, and the algorithm accuracy will also be improved. Thus, the parameter corresponding to this shape ( $\alpha = 5, \beta = 10$ ) meets the requirement of high efficiency, which will be used in the subsequent experiments for adjusting the step factor  $\mu$ .

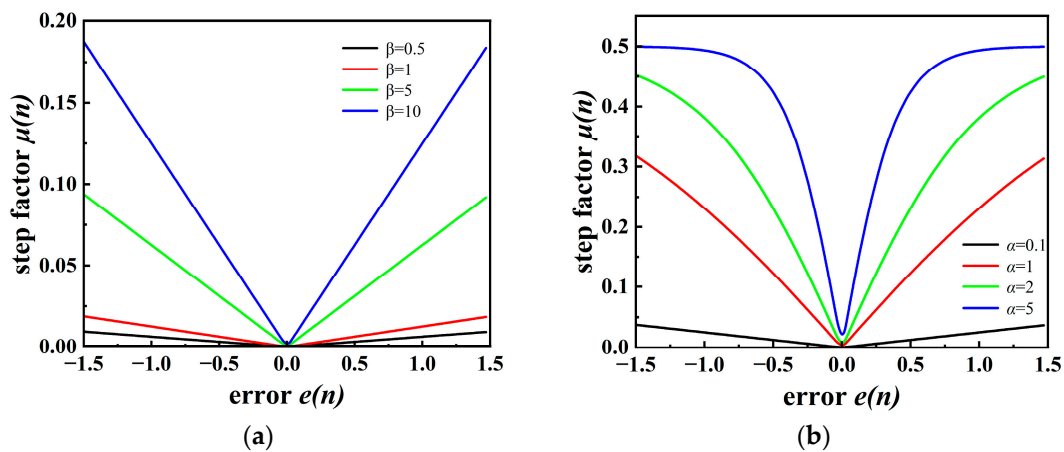


**Figure 4.** Relationship between the error function  $e(n)$  and the step factor  $\mu(n)$ . (a) The factor  $\alpha$  is fixedly set to 0.01, (b) the factor  $\beta$  is fixedly set to 10.

#### 3.2. The Performance of LMS Method for Pulse Compression Signals

A simulation comparison experiment is implemented to verify the advantages of the present method, simulation parameters are shown in detail in Table 1. With the addition of white Gaussian noise (WGN) with the SNR of 5 dB, the RBS signals containing the 128-bit Golay coded signal are simulated, as shown in Figure 5a. It is worth noting that the shape of the coded scattering signal is slowly enhanced along the optical fiber to reach the maximum value and then gradually decreases. The coded pulse sequence does not enter the optical fiber in its entirety at the beginning, but enters gradually so that the scattering power is slowly strengthened until the pulse sequence enters in its entirety, at which point

the scattering power reaches its maximum. Similarly, when the sequence gradually exits the optical fiber, the scattered power decreases slowly. The signal is then filtered using the Hilbert transform with low-pass filtering in Figure 5b. Matched filtering is performed based on the modulated signal. In order to avoid the weak target being masked by adjacent noise due to the sidelobe problem, the prominence of the main peak is measured by the peak sidelobe ratio (PSLR), which can be expressed as:

$$PSLR = 10 * \log_{10} \left( \frac{I_s}{I_m} \right), \tag{13}$$

where  $I_s$  is the peak value of the first sidelobe and  $I_m$  is the peak value of the main lobe.

**Table 1.** Simulation parameter list.

Parameter	Value
Number of LMS filter orders	16
Number of the Golay code (bit)	128
The $\mu$ of WGN	0
The $\sigma$ of WGN	0.1
The SNR of WGN (dB)	5
The length of fiber (km)	9
Number of sampling points	$6.4 \times 10^6$

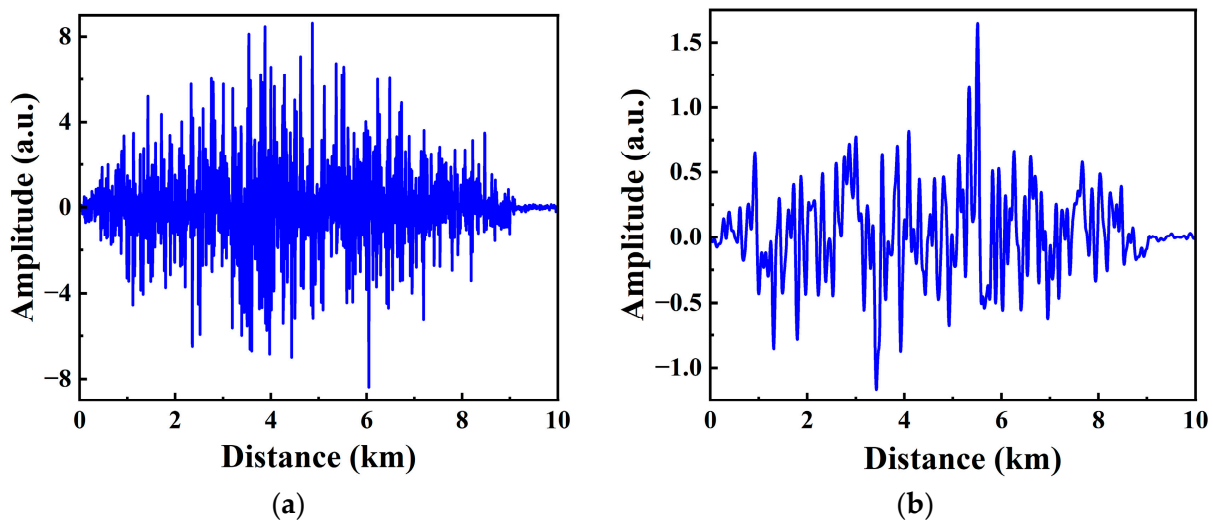


**Figure 5.** RBS signals of 9 km fiber. (a) The raw RBS signals (including Golay codes), (b) the signal after low-pass filter.

To further explore the properties of this algorithm, the method of adding the Hanning window and the method based on the RLS algorithm are compared with the LMS adaptive filtering method, respectively. The flowcharts of three algorithms are shown in Figure 6. The acquired RBS signal is regarded as the input signal  $s(n)$ , and the coded pulse sequence is used as the desired signal  $d(n)$ , which achieves noise reduction and sidelobe suppression through the convergence of the error function. The results of the single-impulse response are shown in Figure 7. The noise and sidelobes of a raw pulse-compressed signal (method A) are evident. Although the method B of adding a Hanning window smooths out the partial noise, the main lobe is widened and the overall curve tends to be a rising cosine. After the RLS algorithm (method C), the PSLR of the signal gains 4.9 dB. The sidelobes close to the main lobe are suppressed, but due to the lack of past observations, a local convergence arose. The sidelobes of the signal after the LMS adaptive filter (method D) is effectively suppressed

and the PSLR can reach  $-19.4$  dB, which is the lowest of the three methods. It demonstrates that the LMS method can reduce noise without increasing extra spatial resolution.

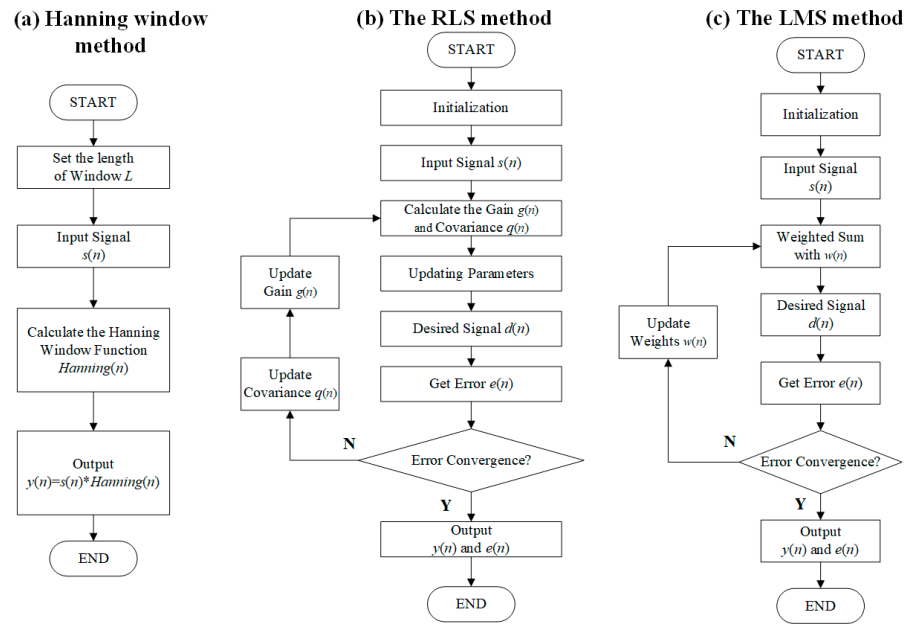


**Figure 6.** Flow charts of (a) the Hanning window method (\* denotes the time-domain multiplication), (b) the RLS method, and (c) the LMS method.

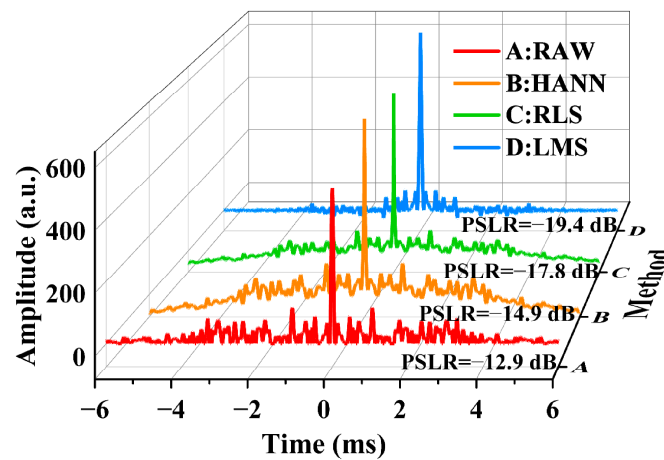


**Figure 7.** Comparison of three filtering algorithms.

## 4. Experiments

### 4.1. Experimental Setup

The coherent  $\Phi$ -OTDR sensing system is employed in the experiments, as shown in Figure 8. The high-coherent light, emitted by a 1550 nm narrow-linewidth laser with the line-width of  $<10$  kHz and the maximum output power of 12 mW, is divided into two parts of 90:10. The light of the 90% part is modulated by an EOM (MPZ-LN-10, iXblue, Paris, France) and then the first erbium-doped fiber amplifier (EDFA) is applied to compensate the loss of light power. The light after coding is chopped by an AOM (T-M080-0.4C2J-3-F2P, Gooch&Housego, Somerset, England) with a frequency shift of 80 MHz into the probe pulses, which are then amplified by the second EDFA and connected with an optical bandpass filter. The role of the optical filter is mainly to filter the amplified spontaneous emission (ASE) noise in the optical amplifier to increase the SNR of EDFA. The arbitrary function generator (AFG) generates two modulation signals, one transmits a two-phase

encoded Golay sequence to the EOM with a single code length of 40 ns, and the other transmits a 1 kHz repetition frequency, single-cycle square wave pulse with a duration of 5.12  $\mu$ s to the AOM.

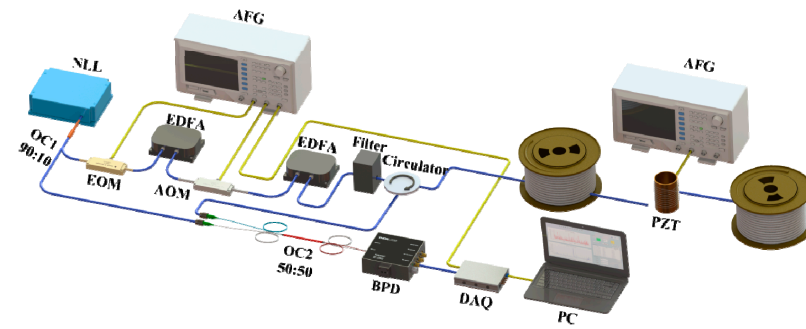


**Figure 8.** The experimental setup of the coherent  $\Phi$ -OTDR sensing system.

A sinusoidal voltage signal is continuously applied to the piezoelectric ceramic transducer (PZT), which is used to simulate the perturbation. The amplified probe pulses are launched into the 11 km fiber under test (FUT) through a circulator. The Rayleigh scattering phenomenon occurs in the FUT, and the RBS light which carries the sensing information returns to a balanced photodetector (BPD) by the circulator. The BPD is used to receive beat frequency signals, and the output is collected by a data acquisition card (DAQ) with a sampling rate of 250 MS/s. Finally, the demodulation is completed on a personal computer (PC). The hardware environment used for data processing was a PC with an AMD Ryzen 7 4800H CPU @ 2.90 GHz, a 16 GB RAM, and an NVIDIA RTX2060 GPU. The software environment is a Windows 11 operating system.

#### 4.2. Parameter Optimisation

Previous simulations have shown that the constant  $\alpha$  may affect the convergence speed and steady state error of the LMS algorithm to a large extent, and the setting of the key parameters needs real data to be verified. Factor  $\alpha$  was set to 1, 2, and 5, respectively, and factor  $\beta$  was fixed to 1. The other parameters were kept constant and processed on the same signals. The relationship between the number of iterations and the error is shown in Figure 9. The fastest convergence and the lowest error are observed when  $\alpha = 5$ , which is consistent with the conclusion of the previous simulation design. When the number of iterations reaches 300, the algorithm converges and approaches the steady state, at which time the MSE drops to below  $-25$  dB; when the number of iterations exceeds 400, the MSE changes by a tiny amount. Since the number of iterations can be set manually, unnecessary computing time is reduced by changing the number of iterations.

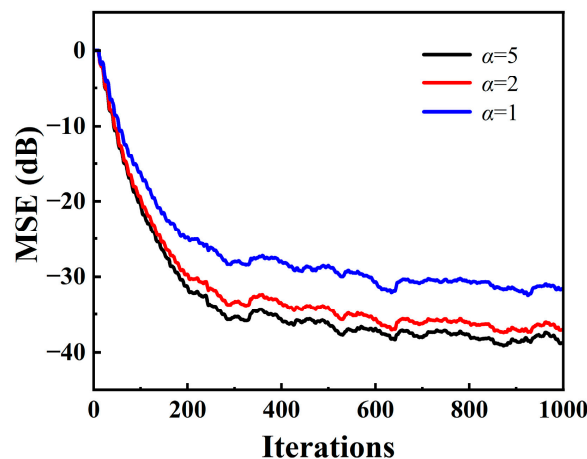


**Figure 9.** The relationship between MSE and number of iterations.

### 5. Discussion of Results

Vibrations are simulated using a PZT wrapped around an 11 km long optical fiber and a sinusoidal signal with a fixed frequency of 200 Hz and an amplitude of 3 V is applied. The PZT is placed at nearly 10,018 m of the 11 km.

In order to verify the superiority of the LMS algorithm proposed in this work, the raw pulse-compressed signal, which is not processed by any filtering algorithm, is compared with the signals processed using three different filtering algorithms in this experiment; i.e., the Hanning window algorithm, the RLS algorithm, and the LMS algorithm. The three main performance indicators (PSLR, spatial resolution and time cost) of different algorithms are statistically presented in Table 2.

**Table 2.** Performance condition data.

Method	PSLR (dB)	Spatial Resolution (m)	Time Cost (s)
Raw signals	−11.60	4.18	0.67
Hanning windows method	−15.32	7.76	1.78
The RLS method	−13.45	5.38	2.32
The proposed method	−15.86	3.81	1.56

The localization results using three filtering algorithms are shown in Figure 10 (the spatial resolution is obtained by measuring the full width at half maximum (FWHM) of the main lobe).

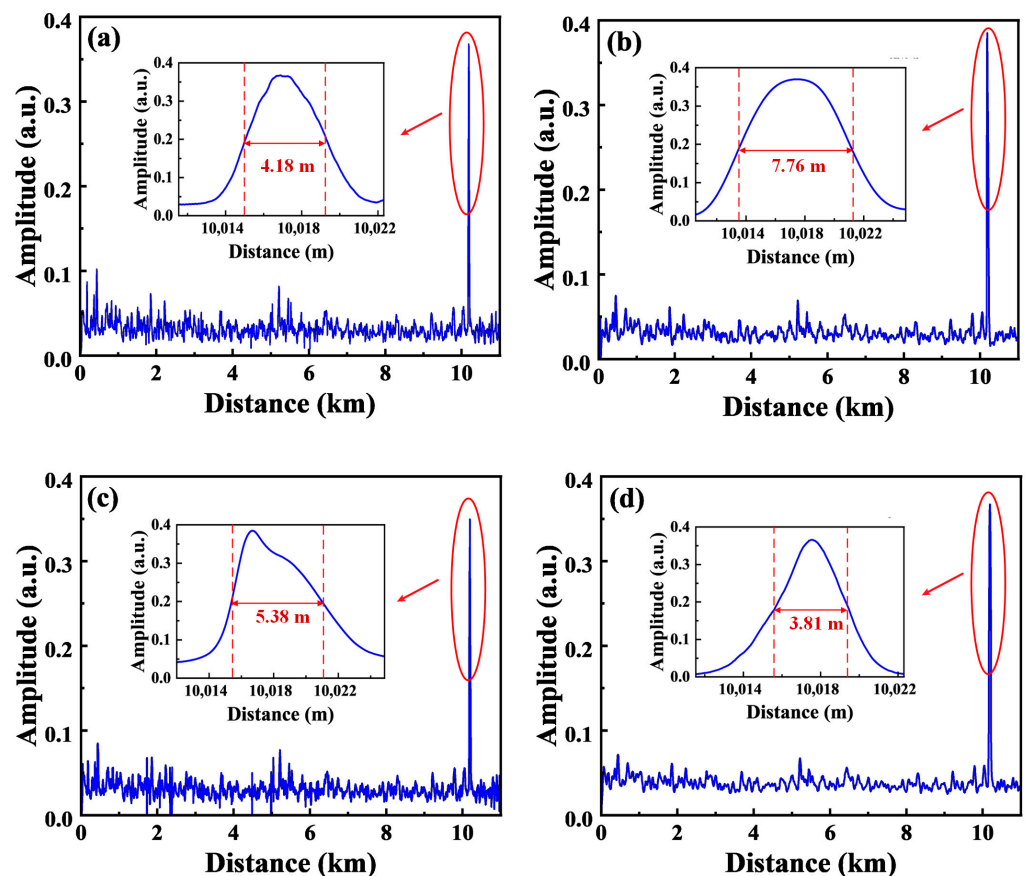


**Figure 10.** Demodulated amplitude localization curves of three filtering algorithms. (a) Raw demodulated curves without any filtering algorithms, (b) based on the Hanning window algorithm, (c) based on the RLS algorithm, and (d) based on the LMS algorithm.

The algorithm based on the Hanning window can be regarded as the summation of the spectra of the three rectangular time windows. The spectral window is shifted by  $\pi/T$  ( $T$  is the period of the signal to be processed) to the left and to the right, so that the sidelobes cancel each other out, eliminating high-frequency interferences and energy leakage. As shown in Figure 10b, the Hanning window method enhances the distinction between signal and noise. For example, near 300 m, the noise caused by the side lobe crosstalk is effectively reduced and the high-frequency component of the overall noise is filtered out. The demodulated pulse width is increased by about 1.8 times due to the widening of the frequency spectrum. In the experiments of the RLS algorithm, its filter order was set to 2. If the filter order is higher, then the convergence becomes slower, and the tracking performance becomes worse, which finally may lead to signal distortion. As shown in Figure 10c, the sidelobe suppression of the RLS algorithm is poorer than the other two filtering algorithms, which may be attributed to the fact that RLS requires using a small period of observation data to estimate the required filter coefficients. Moreover, the vibration signals in the OTDR system tend to be non-stationary signals, which means that the RLS is less effective in filtering the non-stationary signals.

The LMS algorithm differs from the RLS algorithm in that it uses instantaneous values to estimate the correlation matrix and the gradient. It has been shown in adaptive echo cancellation applications that the LMS algorithm can be significantly effective in processing non-smooth signals. Compared to the other two filtering algorithms, the LMS algorithm has the best ability of sidelobe suppression, and its filtering results are shown in Figure 10d. Its PSLR can be up to  $-15.86$  dB, which is 3.7 dB lower than that of the raw signal, showing the potential of the LMS algorithm for sidelobe suppression.

In order to evaluate the stability and real-time performance of the algorithms, the average MSE of the three filtering algorithms is compared with the time cost, as shown in Figures 11 and 12, which is obtained by averaging the results over 200 accumulations. The LMS algorithm has the lowest MSE, which indicates a better stability of error convergence. The RLS algorithm has the worst MSE values, because the RLS is more sensitive to outliers and may not be suitable for processing non-stationary signals. Despite the fastest convergence of RLS, in terms of time cost, the RLS algorithm has the longest total running time due to the highest algorithmic complexity, whereas the LMS and Hanning Window methods consume close to the same amount of time and are more suitable for real-time detection applications.

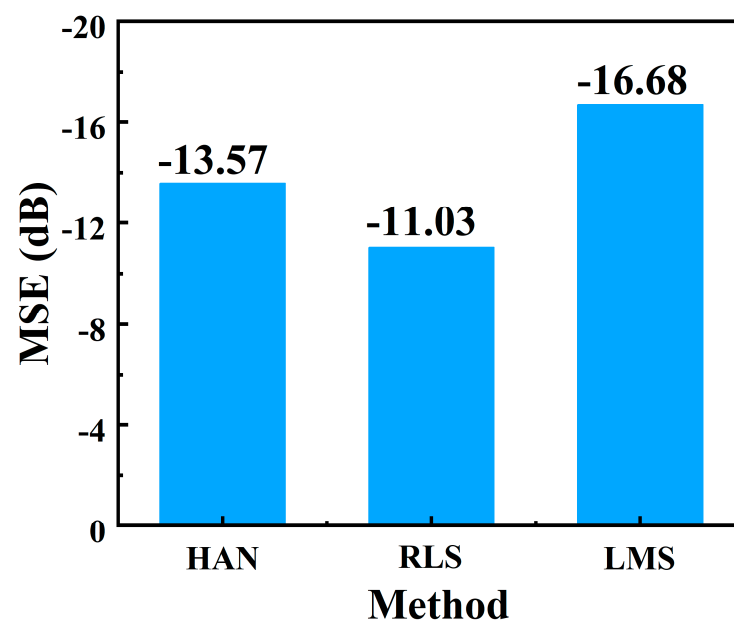


Figure 11. Comparison of MSE for three algorithms.

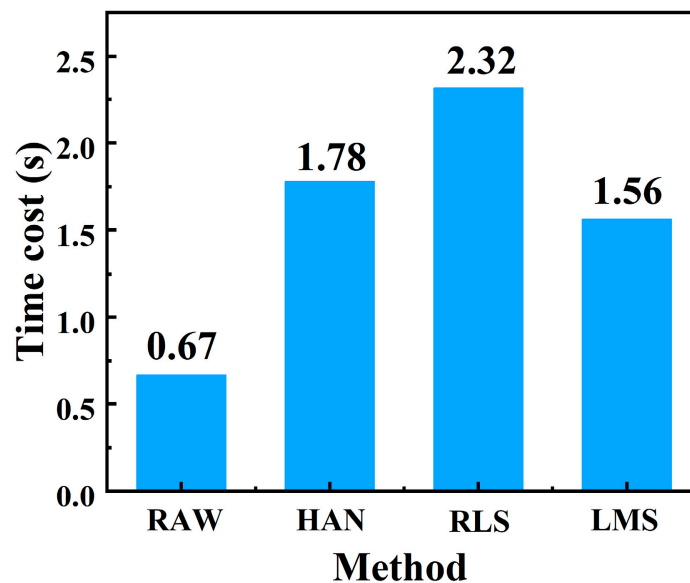


Figure 12. Average running time of the algorithms.

## 6. Conclusions

In this work, a concise adaptive filtering algorithm is proposed for sidelobe suppression in PC-OTDR systems. The algorithm is easy to implement, robust to parameter variations, and suitable for online processing. Simulation experiments demonstrate the effectiveness of the method to eliminate the sidelobes, and experiments based on real data verify that the method can accurately detect and locate vibrations up to 3.81 m spatial resolution at 10 km, with a minimum PSLR of  $-15.86$  dB.

**Author Contributions:** Conceptualization, W.S., Y.H. and X.C.; methodology, X.C.; software, C.D.; validation, C.D., X.C., C.H. and W.S.; formal analysis, W.S. and X.H.; investigation, J.W. and L.L.; resources, W.S., Y.Z. and X.H.; data curation, X.C. and C.H.; writing—original draft preparation, W.S.; writing—review and editing, W.S., X.C. and Y.H.; visualization, Y.Z.; supervision, W.S. and Y.Z.; project administration, X.H. and J.W. All authors have read and agreed to the published version of the manuscript.

**Funding:** This research was funded by the Science and Technology Project of State Grid Jiangsu Electric Power Co., Ltd. (J2022101).

**Institutional Review Board Statement:** Not applicable.

**Informed Consent Statement:** Not applicable.

**Data Availability Statement:** Data underlying the results presented in this paper are not publicly available at the time of publication, but may be obtained from the authors upon reasonable request.

**Conflicts of Interest:** Authors Mr. Wei Shen, Mr. Yong Zhang, Ms. Xin Hu, Mr. Jian Wu and Mrs. Lijun Liu were employed by the company China State Grid Taizhou Power Supply Company. The remaining authors declare that the research was conducted in the absence of any commercial or financial relationships that could be construed as a potential conflict of interest.

## References

- Huang, Y.; Li, Y.; Chen, X.; Dai, J.; Chen, L.; Hu, C.; Deng, C.; Zhang, Q.; Pang, F.; Zhang, X.; et al. Concise method for high-precision vibration recovery of  $\Phi$ -OTDR based on the GF-FastICA algorithm. *Opt. Lett.* **2023**, *48*, 251–254. [[CrossRef](#)] [[PubMed](#)]
- Catalano, E.; Coscetta, A.; Cerri, E.; Cennamo, N.; Zeni, L.; Minardo, A. Automatic traffic monitoring by  $\Phi$ -OTDR data and Hough transform in a real-field environment. *Appl. Opt.* **2021**, *60*, 3579. [[CrossRef](#)] [[PubMed](#)]
- Ding, Z.; Zhang, X.; Zou, N.; Song, J.; Fang, X.; Zhang, Y.  $\Phi$ -OTDR based on-line monitoring of overhead power transmission line. *J. Light. Technol.* **2021**, *39*, 5163–5169. [[CrossRef](#)]

4. Kong, Y.; Liu, Y.; Shi, Y.; Ansari, F.; Taylor, T. Research on the  $\Phi$ -OTDR fiber sensor sensitive for all of the distance. *Opt. Commun.* **2018**, *407*, 148–152. [[CrossRef](#)]
5. Loayssa, A.; Sagues, M.; Eyal, A. Phase noise effects on phase-sensitive OTDR sensors using optical pulse compression. *J. Light. Technol.* **2021**, *40*, 2561–2569. [[CrossRef](#)]
6. Pastor-Graells, J.; Cortés, L.R.; Fernández-Ruiz, M.R.; Martins, H.F.; Azaña, J.; Martin-Lopez, S.; Gonzalez-Herraez, M. SNR enhancement in high-resolution phase-sensitive OTDR systems using chirped pulse amplification concepts. *Opt. Lett.* **2017**, *42*, 1728–1731. [[CrossRef](#)] [[PubMed](#)]
7. Chen, Y.; Fu, Y.; Wang, Z. Distributed fiber birefringence measurement using pulse-compression  $\Phi$ -OTDR. *Photonic Sens.* **2021**, *11*, 402–410. [[CrossRef](#)]
8. Xu, N.; Wang, P.; Wang, Y.; Liu, X.; Bai, Q.; Gao, Y. Crosstalk Noise Suppressed for Multi-frequency  $\Phi$ -OTDR Using Compressed Sensing. *J. Light. Technol.* **2021**, *39*, 7343–7350. [[CrossRef](#)]
9. Jones, M.D. Using simplex codes to improve OTDR sensitivity. *IEEE Photonics Technol. Lett.* **1993**, *5*, 822–824. [[CrossRef](#)]
10. Lee, D.; Yoon, H.; Kim, P.; Park, J.; Kim, N.Y.; Park, N. SNR enhancement of OTDR using biorthogonal codes and generalized inverses. *IEEE Photonics Technol. Lett.* **2004**, *17*, 163–165.
11. Sagues, M.; Piñeiro, E.; Cerri, E.; Minardo, A.; Eyal, A.; Loayssa, A. Two-wavelength phase-sensitive OTDR sensor using perfect periodic correlation codes for measurement range enhancement, noise reduction and fading compensation. *Opt. Express* **2021**, *29*, 6021–6035. [[CrossRef](#)]
12. Zhang, P.; Feng, Q.; Li, W.; Zheng, Q.; Wang, Y. Simultaneous OTDR dynamic range and spatial resolution enhancement by digital LFM pulse and short-time FrFT. *Appl. Sci.* **2019**, *9*, 668. [[CrossRef](#)]
13. Wang, Z.; Zhang, B.; Fu, Y.; Lin, S.; Jiang, J.; Rao, Y. Distributed acoustic sensing based on pulse-coding phase-sensitive OTDR. *IEEE Internet Things* **2018**, *6*, 6117–6124. [[CrossRef](#)]
14. Vazquez, G.D.B.; Martínez, O.E.; Kunik, D. Distributed temperature sensing using cyclic pseudorandom sequences. *IEEE Sens. J.* **2016**, *17*, 1686–1691. [[CrossRef](#)]
15. Mao, Y.; Dai, Z.; Zhang, X. Pulse-coded optical time-domain reflectometer technology. *Laser J.* **2013**, *34*, 42–43.
16. Cui, K.; Liu, F.; Wang, K.; Liu, X.; Yuan, J.; Yan, B.; Zhou, X. Interference-fading-suppressed pulse-coding  $\Phi$ -OTDR using spectrum extraction and rotated-vector-sum method. *IEEE Photonics J.* **2021**, *13*, 6800206. [[CrossRef](#)]
17. Martins, H.F.; Shi, K.; Thomsen, B.C.; Martin-Lopez, S.; Gonzalez-Herraez, M.; Savory, S.J. Real time dynamic strain monitoring of optical links using the backreflection of live PSK data. *Opt. Express* **2016**, *24*, 22303–22318. [[CrossRef](#)] [[PubMed](#)]
18. Shiloh, L.; Levanon, N.; Eyal, A. Highly-sensitive distributed dynamic strain sensing via perfect periodic coherent codes. In Proceedings of the 26th International Conference on Optical Fiber Sensors, OSA Technical Digest, Lausanne, Switzerland, 24–28 September 2018; Optica Publishing Group: Washington, DC, USA, 2018; paper TuE25.
19. Wang, Y.; Jiang, Z. Application of Golay codes to distributed optical fiber sensor for long-distance oil pipeline leakage and external damage detection. *Chin. Opt. Lett.* **2006**, *4*, 141–144.
20. Chen, Y.; Tian, J.; Liu, Y. Variable step size LMS algorithm based on modified Sigmoid function. In Proceedings of the 2014 International Conference on Audio, Language and Image Processing, Shanghai, China, 7–9 July 2014; pp. 627–630.

**Disclaimer/Publisher’s Note:** The statements, opinions and data contained in all publications are solely those of the individual author(s) and contributor(s) and not of MDPI and/or the editor(s). MDPI and/or the editor(s) disclaim responsibility for any injury to people or property resulting from any ideas, methods, instructions or products referred to in the content.